The Astrophysical Journal, 652:313–322, 2006 November 20
© 2006. The American Astronomical Society. All rights reserved. Printed in U.S.A.

# THE FIRST DIRECT DISTANCE DETERMINATION TO A DETACHED ECLIPSING BINARY IN M33[1]

A. Z. Bonanos,[2] K. Z. Stanek,[3] R. P. Kudritzki,[4] L. M. Macri,[5,6] D. D. Sasselov,[7] J. Kaluzny,[8] P. B. Stetson,[9] D. Bersier,[10] F. Bresolin,[4] T. Matheson,[5] B. J. Mochejska,[8] N. Przybilla,[4,11] A. H. Szentgyorgyi,[7] J. Tonry,[4] and G. Torres[7]

*Received 2006 June 11; accepted 2006 July 26*

## ABSTRACT

We present the first direct distance determination to a detached eclipsing binary in M33, which was found by the DIRECT Project. Located in the OB 66 association at coordinates $(\alpha, \delta) = (01^h33^m46^s.17, +30^\circ44'39''.9)$ for J2000.0, it was one of the most suitable detached eclipsing binaries found by DIRECT for distance determination, given its apparent magnitude and orbital period. We obtained follow-up $BV$ time-series photometry, $JHK_s$ photometry, and optical spectroscopy from which we determined the parameters of the system. It contains two O7 main-sequence stars, with masses of $33.4 \pm 3.5$ and $30.0 \pm 3.3\ M_\odot$ and radii of $12.3 \pm 0.4$ and $8.8 \pm 0.3\ R_\odot$, respectively. We derive temperatures of $37{,}000 \pm 1500$ and $35{,}600 \pm 1500$ K. Using $BVRJHK_s$ photometry for the flux calibration, we obtain a distance modulus of $24.92 \pm 0.12$ mag ($964 \pm 54$ kpc), which is $\sim$0.3 mag longer than the Key Project distance to M33. We discuss the implications of our result and the importance of establishing M33 as an independent rung on the cosmological distance ladder.

*Subject headings:* binaries: eclipsing — binaries: spectroscopic — distance scale — galaxies: individual (M33) — stars: fundamental parameters

*Online material:* color figures, machine-readable tables

## 1. INTRODUCTION

Starting in 1996 we undertook a long-term project, DIRECT (i.e., "direct distances"), to obtain the distances to two important galaxies in the cosmological distance ladder, M31 and M33. These direct distances are obtained by measuring the absolute distance to detached eclipsing binaries (DEBs).

M31 and M33 are the nearest and most suitable Local Group galaxies for calibrating the extragalactic distance scale. However, they present a much greater observational challenge than the current anchor of the distance scale, the Large Magellanic Cloud (LMC). Their greater distance makes the brightest stars in them appear $\sim$6 mag fainter than the brightest LMC stars, thus pushing the limit of current spectroscopic capabilities. In addition, crowding and blending become more significant with increasing distance (Mochejska et al. 2000, 2001c). Unfortunately, distances are now known to no better than 10%–15%, as there are discrepancies of 0.2–0.3 mag between various distance indicators (e.g., Benedict et al. 2002; Fig. 8). These uncertainties limit the calibration of stellar luminosities and population synthesis models for early galaxy formation and evolution.

DEBs have the potential to establish distances to M31 and M33 with an unprecedented accuracy of 5% (for reviews and history of the method, see Andersen 1991; Hilditch 1996; Paczynski 1997; Kruszewski & Semeniuk 1999). They offer a single-step distance determination to nearby galaxies and may therefore provide an accurate zero-point calibration of various distance indicators—a major step toward very accurate and independent determination of the Hubble constant. In the last few years, eclipsing binaries have been used to obtain accurate distance estimates to the LMC (e.g., Guinan et al. 1998; Fitzpatrick et al. 2003), the Small Magellanic Cloud (Harries et al. 2003; Hilditch et al. 2005), and most recently to a semidetached system in M31 (Ribas et al. 2005). Distances to individual eclipsing binaries in the Magellanic Clouds are claimed to be accurate to better than 5%.

Detached eclipsing binaries have yet to be used as distance indicators to M31 and M33. The DIRECT project has initiated a search for DEBs and new Cepheids in the M31 and M33 galaxies. We have analyzed five $11' \times 11'$ fields in M31, A–D and F (Kaluzny et al. 1998, 1999; Stanek et al. 1998, 1999; Mochejska et al. 1999), and one $22' \times 22'$ field, Y (Bonanos et al. 2003). A total of 674 variables, mostly new, were found: 89 eclipsing binaries, 332 Cepheids, and 253 other periodic, possible long-period or nonperiodic variables. We have analyzed two fields in M33, A and B (Macri et al. 2001, hereafter Paper VI) and found 544 variables: 47 eclipsing binaries, 251 Cepheids, and 246 other variables. Follow-up observations of fields M33A and M33B produced 280 and 612 new variables, respectively (Mochejska et al. 2001a, hereafter Paper VII; Mochejska et al. 2001b), including 101 new eclipsing binaries. Variables from two more DIRECT fields, one in M31 and the other in M33, remain to be reported.

[1] Based on observations obtained with 1.2 m FLWO, 2.1 m KPNO, 3.5 m WIYN, 8 m Gemini, and 10 m Keck II telescopes.

[2] Vera Rubin Fellow, Department of Terrestrial Magnetism, Carnegie Institution of Washington, 5241 Broad Branch Road NW, Washington, DC 20015; bonanos@dtm.ciw.edu.

[3] Department of Astronomy, Ohio State University, 140 West 18th Avenue, Columbus, OH 43210; kstanek@astronomy.ohio-state.edu.

[4] Institute for Astronomy, University of Hawaii, 2680 Woodlawn Drive, Honolulu, HI 96822; kud@ifa.hawaii.edu, bresolin@ifa.hawaii.edu, jt@ifa.hawaii.edu.

[5] National Optical Astronomy Observatory, 950 North Cherry Avenue, Tucson, AZ 85719; lmacri@noao.edu, matheson@noao.edu.

[6] Hubble Fellow and Goldberg Fellow.

[7] Harvard-Smithsonian Center for Astrophysics, 60 Garden Street, Cambridge, MA 02138; sasselov@cfa.harvard.edu, aszentgyorgyi@cfa.harvard.edu, torres@cfa.harvard.edu.

[8] Copernicus Astronomical Center, Bartycka 18, 00-716 Warsaw, Poland; jka@camk.edu.pl, mochejsk@camk.edu.pl.

[9] National Research Council of Canada, Herzberg Institute of Astrophysics, 5071 West Saanich Road, Victoria, BC V9E 2E7, Canada; peter.stetson@nrc-cnrc.gc.ca.

[10] Liverpool John Moores University, Twelve Quays House, Egerton Wharf, Birkenhead, CH41 1LD, UK; dbf@astro.livjm.ac.uk.

[11] Dr. Remeis-Sternwarte, Astronomical Institute of the University of Erlangen-Nuremberg, Sternwartstrasse 7, D-96049 Bamberg, Germany; przybilla@sternwarte.uni-erlangen.de.

TABLE 1
*V*-Band DEB Light Curve

| HJD[a] | *V* | $\sigma_{mag}$ |
|---|---|---|
| 1451.6862..... | 19.654 | 0.007 |
| 1451.6979..... | 19.630 | 0.008 |
| 1451.7073..... | 19.612 | 0.008 |
| 1451.7241..... | 19.602 | 0.008 |
| 1451.7329..... | 19.601 | 0.008 |

Note.—Table 1 is published in its entirety in the electronic edition of the *Astrophysical Journal*. A portion is shown here for guidance regarding its form and content.
[a] HJD −2,450,000.

TABLE 2
*B*-Band DEB Light Curve

| HJD[a] | *B* | $\sigma_{mag}$ |
|---|---|---|
| 1451.7623..... | 19.376 | 0.010 |
| 1451.8347..... | 19.356 | 0.009 |
| 1451.8981..... | 19.338 | 0.007 |
| 1452.8169..... | 19.314 | 0.008 |
| 1452.8922..... | 19.321 | 0.008 |

Note.—Table 2 is published in its entirety in the electronic edition of the *Astrophysical Journal*. A portion is shown here for guidance regarding its form and content.
[a] HJD −2,450,000.

Of the 237 eclipsing binaries found by DIRECT, only four are bright enough ($V_{max} < 20$ mag) for distance determination with currently available telescopes. An additional criterion for selection is that they contain deep eclipses, which removes degeneracies in the modeling. D33 J013346.2+304439.9 is the brightest of these, discovered in field M33A (Paper VI), and this paper presents the distance we obtained to it with subsequent observations. In § 2 we describe the observations and the data reduction; in § 3 we present the light-curve and radial velocity curve analysis, in § 4 the distance determination, and in § 5 the discussion.

## 2. OBSERVATIONS

The DIRECT Project discovered the detached eclipsing binary D33 J013346.2+304439.9 ($\alpha = 01^h33^m46^s.17$, $\delta = +30°44'39''.9$; J2000.0) in field M33A (Paper VI), using the F. L. Whipple Observatory 1.2 m telescope between 1996 September and 1997 October.

### 2.1. *Follow-up V- and B-Band Photometry*

In 1999 and 2001 we obtained follow-up photometry with the Tektronix 2048 × 2048 CCD (T2KA camera) at the Kitt Peak National Observatory (KPNO) 2.1 m telescope, with a pixel scale of 0.″305 pixel$^{-1}$. The 1999 observations are described in Paper VII. In addition we obtained 94 × 600 s exposures in the *V* band and 19 × 600 s in *B* band in 2001 October. Tables 1 and 2 present the *BV* light curves. The images were processed with standard IRAF routines.[12] The nonlinearity of the CCD was corrected with the method outlined in Paper VII.

The photometry for the variable stars was extracted using the ISIS image subtraction package (Alard & Lupton 1998; Alard 2000) from the *V*- and *B*-band data. We followed the ISIS reduction procedure described in detail in Paper VII. DAOPHOT/ALLSTAR PSF photometry was performed on the *B* and *V* reference image separately, and aperture corrections were applied before converting the flux light curves to instrumental magnitudes. In addition, we performed DAOPHOT PSF photometry on all frames to verify that the shapes of the light curves were correctly measured with ISIS.

Observations of the DEB were also obtained with the Mini-Mosaic CCD camera on the WIYN[13] 3.5 m telescope at KPNO, with a pixel scale of 0.″28 pixel$^{-1}$. On 1999 October 3, we obtained a 300 s exposure in each of the *V* and *B* bands at air mass 1.28 and 1.25, respectively, and at phase 0.73. Conditions were photometric, and three Landolt standard fields were observed, covering a range in air mass from 1.17 to 1.40. These data were used for calibrating the *BV* light curves to standard photometric bands (Landolt 1992).

### 2.2. *Photometric Calibration*

The aperture photometry of the stars in the Landolt (1992) fields was derived with DAOGROW (Stetson 1990). The photometric solutions were very robust (rms ∼ 0.03 mag). Instrumental magnitudes were derived with DAOPHOT/ALLSTAR and aperture corrections with DAOGROW after subtraction of all but PSF stars. As for standards the largest aperture was set to 24 pixels. The WIYN calibration yielded $V = 19.51 \pm 0.01$ and $B - V = -0.20 \pm 0.01$ mag for the DEB.

Other surveys of M33 have measured photometry for the DEB: Massey et al. (1996; star UIT 196) and Ivanov et al. (1993; star 929); however, the quality of the data is inferior. The Local Group Survey (Massey et al. 2006) has obtained high-quality photometry of the DEB, using the KPNO 4 m telescope. They measured out of eclipse magnitudes of $V = 19.52 \pm 0.01$, $B - V = -0.20 \pm 0.01$, $U - B = -1.14 \pm 0.01$, $V - R = -0.12 \pm 0.01$, and $R - I = -0.18 \pm 0.01$, in excellent agreement with our *BV* values. Henceforth, we use the average of these values: $B = 19.32 \pm 0.01$ and $V = 19.52 \pm 0.01$.

### 2.3. *Near-Infrared Photometry*

We carried out near-infrared observations of the DEB using the Gemini North telescope and NIRI (Hodapp et al. 2003), as queue program GN-2005B-DD-4. We observed the system in the *J*, *H*, and $K_s$ bandpasses on 2006 January 3 (UT) between phases 0.39–0.40. Conditions were photometric and the range of air masses was between 1.05 and 1.25. The typical PSF FWHM was 0.″3, or 2.5 pixels at the f/6 plate scale of NIRI. Total on-source exposure times were 11 minutes in *J*, 35 minutes in *H*, and 32 minutes in $K_s$, with individual exposures of 30 s in *J* and *H* and 60 s in $K_s$.

We reduced the images (bad pixel masking, dark current correction, sky subtraction, and flat fielding) using the IRAF Gemini NIRI package (ver. 1.8). We performed PSF photometry using DAOPHOT and ALLSTAR (Stetson 1987) on each individual image, because the PSF exhibited significant variations in ellipticity from image to image. We defined the PSF out to a radius of 8 pixels (0.″94), which included essentially all of the stellar flux. Aperture corrections were derived using DAOGROW (Stetson 1990) and amounted to ≲0.02 mag.

[12] IRAF is distributed by the National Optical Astronomy Observatory, which is operated by the Association of Universities for Research in Astronomy (AURA), Inc., under cooperative agreement with the National Science Foundation (NSF).
[13] The WIYN Observatory is a joint facility of the University of Wisconsin-Madison, Indiana University, Yale University, and the National Optical Astronomy Observatory.

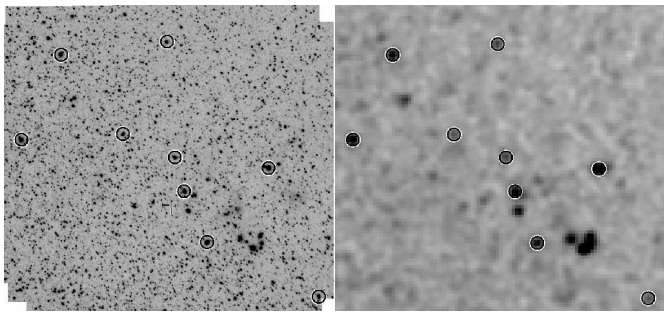


FIG. 1.—$K_s$-band finder chart, $1\farcm8 \times 1\farcm8$; north is up, and east to the left. The circles indicate the stars used for calibration on both the NIRI image (*left*) and the 2MASS image (*right*). The DEB is marked on the NIRI image by the crosshairs.

We calibrated the photometry using several 2MASS stars in the field of view that were determined to be isolated from our higher resolution Gemini images. In some cases, we added the flux of faint neighboring stars to that of the bright comparison star, since they appear unresolved in the 2MASS images. We determined effective zero points for this Gemini NIRI data set (at air mass $\sim$1.1 and $J - K_s \sim 1$) of 23.82, 23.75, and 23.23 $\pm$ 0.05 mag for $J$, $H$, and $K_s$, respectively (corresponding to the 2MASS magnitude of a star that would yield 1 ADU s$^{-1}$). By following this calibration path, we found mean out-of-eclipse magnitudes for the DEB of $J = 20.02 \pm 0.05$, $H = 20.05 \pm 0.06$, and $K_s = 20.13 \pm 0.06$ mag.

Figure 1 is a $K_s$-band finder chart of the field, indicating the location of the DEB and the photometric calibration reference stars in both the Gemini/NIRI and 2MASS images.

### 2.4. *Spectroscopic Observations*

We obtained spectra of the DEB over seven epochs, six half and one full night (2004 October 11 UT), in the fall of 2002, 2003, and 2004 with the Echellette Spectrograph and Imager (ESI; Sheinis et al. 2002) on the 10 m Keck II telescope on Mauna Kea. In the fall of 2004, we also obtained four sets of $5 \times 2700$ s spectra at quadrature with the B1200 line mm$^{-1}$ grating of the Gemini Multi-Object Spectrograph (GMOS; Hook et al. 2003) on the Gemini-North 8 m telescope on Mauna Kea. Table 3 summarizes the exposure times and dates of observations, which total four nights on Keck and 19 hr on Gemini. The ESI spectra range from 3950–10000 Å, have a reciprocal dispersion of 11 km s$^{-1}$ pixel$^{-1}$, and with a $1''$ slit we achieved a velocity resolution of 74 km s$^{-1}$. The GMOS spectra range from 3770–5227 Å, have a 0.23 Å pixel$^{-1}$ dispersion, and with a $0\farcs75$ slit we achieved a resolution of 120 km s$^{-1}$. The signal-to-noise ratio (S/N) of the spectra ranges from 15 to 40. Observations were taken at low air mass and the slit was rotated 75° east from the north to minimize contamination from nearby H II regions.

Standard CCD processing was done with IRAF. We used the algorithm of Pych (2004) for cosmic-ray rejection from each two-dimensional image. We then optimally extracted the spectra and calibrated them in wavelength with IRAF routines. Three copper-argon calibration spectra were interspersed between the five sets of GMOS spectra. In 2002, we found ESI to be stable to a fraction of a pixel; thus, in subsequent runs we only took several CuAr and HgNeXe lamps at the beginning and end of the night (or half night) that we averaged together and used to establish the wavelength solution, with low-order polynomial fits to the lamps. The small spatial extent of the ESI slit made background subtraction difficult at the Balmer lines. Such contamination does not affect the lines used for radial velocity determination, however. Spectra of standard stars were obtained at each epoch with ESI and were used to calibrate the DEB in flux and to remove telluric lines with our IDL routines (Wade & Horne 1988; Matheson et al. 2000).

We used the IRAF Gemini package (ver. 1.7) to reduce the GMOS data. We wavelength-calibrated the three extensions/chips of each exposure separately with copper-argon lamps for a more accurate wavelength calibration and merged the extensions at the end. The gaps between chips correspond to the regions 4244–4255 and 4731–4747 Å in the spectrum. For the flux calibration we used standard star spectra that were observed nearest in time to the DEB. The observations from each night were averaged together, weighting by the exposure times. Finally, we normalized the combined spectra, dividing them by a spline function, which we fit interactively to points in the continuum region.

Absorption lines from both stars are clearly resolved in the spectrum. We were not able to avoid emission from nearby H II regions, and thus our spectra contain strong nebular emission in the hydrogen lines and weaker emission in some of the helium lines, as well as forbidden oxygen lines [O III] $\lambda\lambda$4959, 5007. The GMOS spectra show broad Ca II $\lambda$3933.7 absorption and a narrow absorption line at $\lambda$4433.3, possibly due to an interstellar band.

## 3. LIGHT-CURVE AND RADIAL VELOCITY CURVE ANALYSIS

Initially, we used the multiharmonic analysis of variance technique (Schwarzenberg-Czerny 1989, 1996) to search the light curves for periodicity. We merged the $B$ and $V$ light curves, scaled to $V$, and searched for the best period by fitting a Gaussian to the peak of the periodogram generated by this method, finding a period $P = 4.8935$ days, which serves as the initial guess for

TABLE 3
SPECTROSCOPIC OBSERVATIONS

| UT Observation Date | Telescope | Instrument | Number of Exposures | Total Exposure Time (hr) | Exposure Midpoint (HJD) |
|---|---|---|---|---|---|
| 20021031 | Keck II | ESI | 4 | 1.53 | 2,452,578.8611 |
| 20021101 | Keck II | ESI | 2 | 0.575 | 2,452,579.8873 |
| 20030903 | Keck II | ESI | 5 | 2.92 | 2,452,886.0960 |
| 20030904 | Keck II | ESI | 4 | 3.25 | 2,452,887.0532 |
| 20030905 | Keck II | ESI | 4 | 3.20 | 2,452,888.0598 |
| 20040816 | Gemini | GMOS-N | 5 | 3.75 | 2,453,234.0229 |
| 20040818 | Gemini | GMOS-N | 5 | 3.75 | 2,453,236.0637 |
| 20040912 | Gemini | GMOS-N | 5 | 3.75 | 2,453,261.0327 |
| 20041009 | Gemini | GMOS-N | 5 | 3.75 | 2,453,287.9396 |
| 20041011 | Keck II | ESI | 7 | 5.25 | 2,453,289.9871 |
| 20041112 | Keck II | ESI | 3 | 4.50 | 2,453,321.8224 |

TABLE 4
Heliocentric Radial Velocity Measurements for the DEB

| Exposure Midpoint (HJD) | Orbital Phase | $RV_1$ (km s$^{-1}$) | $RV_2$ (km s$^{-1}$) | $(O-C)_1$ (km s$^{-1}$) | $(O-C)_2$ (km s$^{-1}$) |
|---|---|---|---|---|---|
| 2,452,578.8611 | 0.386 | −430 | −15 | −42 | 7 |
| 2,452,579.8873 | 0.595 | −20 | −560 | −8 | −124 |
| 2,452,886.0960 | 0.167 | −440 | −30 | −35 | −21 |
| 2,452,887.0532 | 0.362 | −415 | 10 | 6 | −4 |
| 2,452,888.0598 | 0.568 | −35 | −320 | 16 | 69 |
| 2,453,234.0229 | 0.260 | −460 | 70 | 5 | 7 |
| 2,453,236.0637 | 0.677 | −25 | −490 | −40 | −25 |
| 2,453,261.0327 | 0.779 | −5 | −445 | 17 | −22 |
| 2,453,287.9396 | 0.278 | −460 | 70 | 8 | 4 |
| 2,453,289.9871 | 0.698 | 5 | −475 | −8 | −7 |
| 2,453,321.8224 | 0.203 | −410 | 55 | 30 | 25 |

the modeling. In this paper we define the primary star (star 1) photometrically, as the hotter star producing the deeper eclipse at phase zero. In the analysis below we show the primary to be the larger and more massive star also.

### 3.1. *Initial Light-Curve Parameter Estimation*

We first estimated the parameters of the $V$-band light curve with the EBOP code (Nelson & Davis 1972; Popper & Etzel 1981). We computed fits for several periods and found the fit with a period of $P = 4.8938$ days to have the smallest residuals. Bootstrap analysis (Press et al. 1992) yielded very small values for the errors, ∼2%, which are smaller than errors from the radial velocity curves discussed later on.

EBOP's biaxial ellipsoidal approximation holds for values of oblateness $\epsilon$ less than 0.04 and fractional radii less than 0.2. We find $\epsilon = 0.02$ but a fractional radius for the primary slight larger than 0.2, and thus we proceed to a more detailed treatment. Using the EBOP parameters as starting values, we fit the 83 $B$-band points and the 278 $V$-band points in the light curve simultaneously with the 2003 April version of the Wilson-Devinney (WD) program (Wilson & Devinney 1971; Wilson 1979, 1990; van Hamme & Wilson 2003) in the detached mode (MODE=2). We found the following best-fit parameters: eccentricity $e = 0.17$, $\omega = 251\overset{\circ}{.}8$, inclination $i = 86\overset{\circ}{.}9$, light ratio $L_2/L_1 = 0.4912$ in $V$ and 0.4923 in $B$, and flux ratio $F_1/F_2 = 1.039$ in $V$ and 1.036 in $B$, in agreement with the definition of the primary being the hotter star. These preliminary values were refined later (see § 3.3) in a simultaneous fit of both light curves and radial velocity curves. In eccentric binaries, there is a degeneracy in determining the radius and luminosity ratio from the light curves alone. We found that reversing the radii so that the primary is smaller and less luminous also produced a good light-curve fit. We resolve this by using the spectroscopic light ratio in § 3.4.

### 3.2. *TODCOR Analysis of Spectra*

We used the method of two-dimensional cross-correlation or TODCOR, developed by Zucker & Mazeh (1994), to measure radial velocities of the stars in the DEB. TODCOR can distinguish small velocity separations even more accurately than one-dimensional cross-correlation. Initially, we calculated a grid of template spectra over a range of temperatures around 30,000 K using the LTE ATLAS9 models and opacities developed by Kurucz (1993). We ran TODCOR with ATLAS9 template spectra and found preliminary values for the semi-amplitudes and mass ratio, and thus the semimajor axis. We thus obtained estimates for $\log(g)$ and the masses from which we computed a grid of nonlocal thermodynamic equilibrium (NLTE) spectra with FASTWIND (Santolaya-Rey et al. 1997; Puls et al. 2005). This hydrodynamic NLTE code includes stellar winds, spherical extension, and metal-line blanketing of millions of lines in (approximate) NLTE. We found the best-fit spectra to have effective temperatures $T_{\rm eff1} = 37{,}000 \pm 1500$ K and $T_{\rm eff2} = 35{,}600 \pm 1500$ K. A detailed description of the temperature determination follows in § 3.4.

The NLTE spectra were used to derive the final radial velocities of the stars. We prepared them for TODCOR by applying rotational broadening of 120 km s$^{-1}$, which was determined from the spectral fits. We also applied instrumental broadening to match the resolution of the observations by convolving the models with a Gaussian of appropriate FWHM for ESI and GMOS. The IRAF `rvsao.xcsao` (Tonry & Davis 1979; Kurtz et al. 1992) task was used to compute the one-dimensional cross-correlation function, required by TODCOR, for each observed spectrum with the appropriate model. We used the range 3975–6000 Å for ESI spectra and 3950–5227 Å for GMOS spectra, excluding the Balmer lines and [O III] emission lines. We ran TODCOR with model spectra containing only hydrogen and helium lines, masking out the broad hydrogen lines and assuming a luminosity ratio $L_2/L_1 = 0.49$ found from the light-curve analysis. Table 4 presents the measured velocities for each spectrum. The spectrum of 20021101 at phase 0.595 produced a spurious velocity for the secondary star. We excluded it from further analysis because this spectrum has the lowest S/N (∼15), and the secondary contributes only half the amount of light to the spectrum, which makes it even harder to measure. The velocities measured are robust and accurate to 30 km s$^{-1}$. As a final test we ran TODCOR using ATLAS9 models [37,000, 36,000 K with $\log(g) = 4$] and TLUSTY (Lanz & Hubeny 2003) models including metals [37,500 K for both stars and $\log(g) = 3.75$ and 4.00]. Both runs produced radial velocities and semi-amplitudes in agreement within errors.

From the radial velocity curve analysis alone, we found a mass ratio $q = M_2/M_1 = 0.90 \pm 0.06$, velocity semi-amplitudes of $K_1 = 240 \pm 11$ and $K_2 = 268 \pm 11$ km s$^{-1}$, systemic velocity $\gamma = -214.1 \pm 6.8$ km s$^{-1}$, and semimajor axis $a \sin i = 48.3 \pm 1.6\ R_\odot$ and minimum masses of $M_1 \sin^3 i = 33.3 \pm 3.5$ and $M_2 \sin^3 i = 29.9 \pm 3.3\ M_\odot$, fixing $e$ and $\omega$ from the preliminary light-curve analysis described above.

Measuring radial velocities of early-type stars is complex for several reasons: they have very few lines, and the strongest of these, mainly the Balmer lines, are broadened due to rotation and the Stark effect. The standard one-dimensional cross-correlation method has been shown to produce systematically smaller semi-amplitudes when blended lines are included. Hilditch (2001) estimates the effect to be ∼50% for hydrogen lines and ∼10%

TABLE 5
RESULTS FROM COMBINED *LC* AND *RV* CURVE ANALYSIS WITH THE WILSON-DEVINNEY PROGRAM

| Parameter | Value |
|---|---|
| Period, $P$ (days) | 4.89380 ± 0.00003 |
| Time of primary eclipse, HJD $_0$ | 2,451,451.4040 (5) |
| Inclination, $i$ (deg) | 87.2 ± 0.5 |
| Eccentricity, $e$ | 0.18 ± 0.02 |
| Longitude of periastron, $\omega$ (deg) | 252.4 ± 1.0 |
| Surface potential, $\Omega_1$ | 5.09 ± 0.03 |
| Surface potential, $\Omega_2$ | 6.29 ± 0.06 |
| Light ratio in $V$, $L_2/L_1$ | 0.492 ± 0.005 |
| Light ratio in $B$, $L_2/L_1$ | 0.493 ± 0.005 |
| Mass ratio, $q$ | 0.91 ± 0.07 |
| Systemic velocity, $\gamma$ (km s$^{-1}$) | −214 ± 7 |
| Semi-major axis, $a(R_\odot)$ | 48.4 ± 1.6 |
| Semi-amplitude, $K_1$ km s$^{-1}$) | 242 ± 11 |
| Semi-amplitude, $K_2$ (km s$^{-1}$) | 266 ± 11 |
| Radius: | |
| $r_{1,\,\mathrm{pole}}$ | 0.248 ± 0.002 |
| $r_{1,\mathrm{point}}$ | 0.267 ± 0.002 |
| $r_{1,\mathrm{side}}$ | 0.252 ± 0.002 |
| $r_{1,\mathrm{back}}$ | 0.261 ± 0.002 |
| $r_1$ [a] | 0.254 ± 0.002 |
| $r_{2,\mathrm{pole}}$ | 0.180 ± 0.002 |
| $r_{2,\mathrm{point}}$ | 0.185 ± 0.002 |
| $r_{2,\mathrm{side}}$ | 0.181 ± 0.002 |
| $r_{2,\mathrm{back}}$ | 0.184 ± 0.002 |
| $r_2$ [a] | 0.182 ± 0.002 |

[a] Volume radius.

for helium lines, for velocity differences between components of less than 200 km s$^{-1}$. However, with TODCOR systematic errors due to blending are avoided. Finally, the rotational velocity used in the synthetic spectrum is also a source of systematic error if it deviates from the true value. The value of $v \sin i$ fit to the spectra is accurate to ∼20 km s$^{-1}$.

We attempted to use the spectral disentangling technique (Simon & Sturm 1994), which has been shown to be superior to standard one-dimensional cross-correlation by Harmanec et al. (1997) in yielding more accurate velocities. We used the public code FDBinary (Ilijic et al. 2001, 2004) but found significantly different semi-amplitudes than those from the TODCOR analysis, with unrealistically small errors, and concluded that higher signal-to-noise spectra (S/N ≥ 40) at all epochs are required for this method to give meaningful results. The presence of nebular emission lines, even though masked out, may also have hindered this method.

### 3.3. *Combined Analysis of LC and RV Curves*

With the radial velocity measurements in hand, we proceeded to perform a simultaneous fit of the *BV* light curves and the radial velocity curves with WD in the detached mode (MODE 2) for 13 parameters: the inclination $i$, eccentricity $e$, the argument of periastron $\omega_0$, the semimajor axis $a$, system center of mass radial velocity $\gamma$, the surface potential for each star $\Omega_1$ and $\Omega_2$, mass ratio $q = M_2/M_1$, $T_{\mathrm{eff}\,2}$, period $P$, time of primary eclipse $T_0$, and bandpass luminosity $L_1$ in each band.

Following the advice of van Hamme (1993) we used the square-root limb darkening law, which gives better results for hot stars in the optical. Theoretical bolometric and passband-specific limb-darkening coefficients were taken from theoretical values from Claret (2000) for a LTE ATLAS9 stellar atmosphere model with $T_{\mathrm{eff}} = 37{,}000$ K, $\log(g) = 4.0$ (cgs), turbulent velocity of 4 km s$^{-1}$, and solar metallicity. We fixed gravity brightening exponents to unity and albedos to 0.5 from theoretical values (Hilditch 2001) for stars at such temperatures. For reflection, we used a MREF value of 1 for simple treatment of reflection with the inverse square law. In addition, we allowed for non-Keplerian effects on the radial velocity curve. All data points were weighted equally.

TABLE 6
DEB PHYSICAL PARAMETERS

| Parameter | Primary | Secondary |
|---|---|---|
| Mass ($M_\odot$) | 33.4 ± 3.5 | 30.0 ± 3.3 |
| Radius ($R_\odot$) | 12.3 ± 0.4 | 8.8 ± 0.3 |
| $\log g$ (cgs) | 3.78 ± 0.03 | 4.03 ± 0.03 |
| $T_{\mathrm{eff}}$ (K) | 37,000 ± 1500 | 35,600 ± 1500 |
| $\log L/L_\odot$ | 5.41 ± 0.17 | 5.05 ± 0.18 |

We defined convergence to be reached after three consecutive iterations for which the corrections for all adjusted parameters were smaller than their respective standard or statistical errors (e.g., Kallrath & Milone 1999). The results of the fit and 1 $\sigma$ errors are given in Table 5, and the derived physical parameters in Table 6. The rms residuals were 0.01 for both $B$ and $V$ light curves. Figures 2 and 3 show the $V$- and $B$-band light-curve model fits for the DEB. Note that the deviation of the secondary eclipse from phase 0.5 is due to the eccentricity of the system. The radial velocity curve is presented in Figure 4. The rms residuals are 26.0 km s$^{-1}$ for the primary and 28.0 km s$^{-1}$ for the secondary star. The ephemeris is

$$T(\mathrm{HJD}) = 2{,}451{,}451.4040(5) + 4.89380(3) \times \mathrm{E}, \quad (1)$$

The stars are nearly spherical; the radius of the primary varies by 2% depending on the direction (toward the pole, inner Lagrangian point, side, back), while the variation in the secondary is less than 1%. We used the volume radius to compute the surface area of the stars for our distance calculation. The WD values yield masses $M_1 = 33.4 \pm 3.5$ and $M_2 = 30.0 \pm 3.3\ M_\odot$, radii

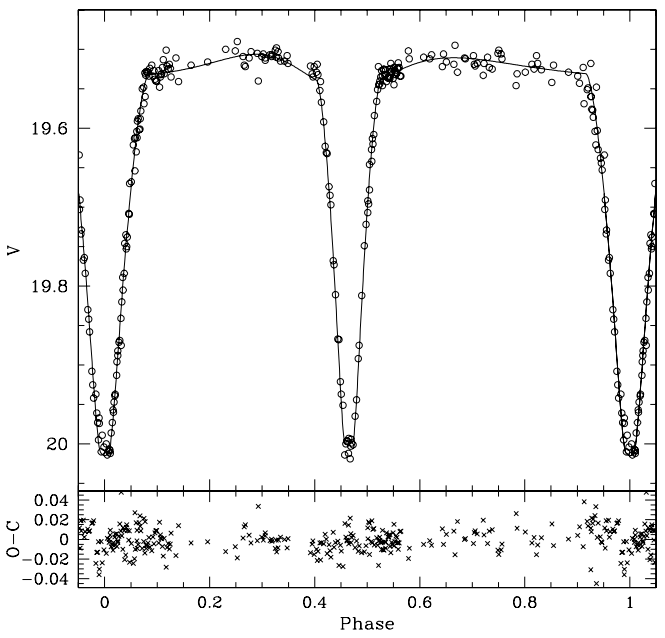



FIG. 2.—$V$-band light curve of the DEB with model fit from the Wilson-Devinney program. The rms is 0.01 mag. [*See the electronic edition of the Journal for a color version of this figure.*]

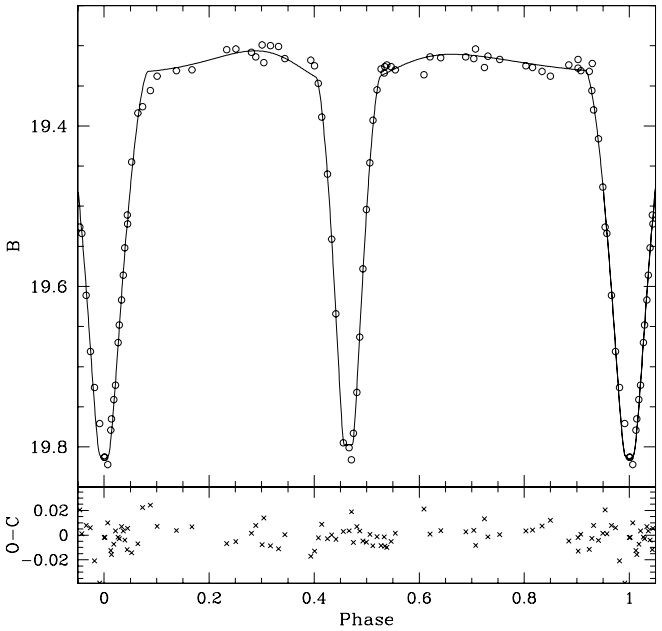



FIG. 3.—Same as Fig. 2, but for the *B* band. [*See the electronic edition of the Journal for a color version of this figure.*]

$R_1 = 12.3 \pm 0.4$ and $R_2 = 8.8 \pm 0.3\ R_\odot$, and values for log ($g$) of 3.78 for the primary and 4.03 for the secondary. The flux ratio derived from the luminosity and radius ratio is $F_1/F_2 = 1.040$ in $V$ band and $F_1/F_2 = 1.047$ in $B$ band. This implies a temperature difference of 1000–1500 K in the temperature range considered and at the gravities of the two objects.

We initially allowed the third light to be a free parameter; however, after converging to negative values, we set it to zero. The presence of deep eclipses also gives us confidence that there is no significant blending/crowding effect present. We fixed $d\omega/dt$ to zero, since the residuals did not reveal any significant trend from the 2 year baseline of our photometry.

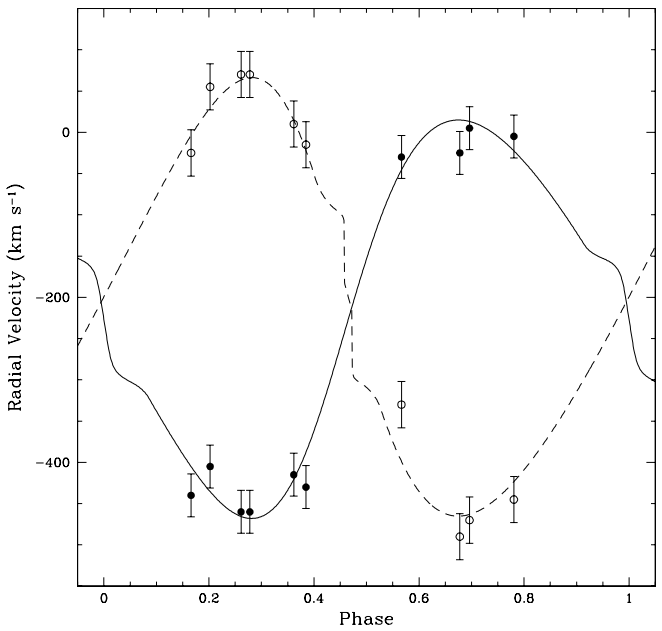



FIG. 4.—Radial velocities for the DEB measured by TODCOR with FASTWIND synthetic spectra. The model fit is from Wilson-Devinney program, including the Rossiter effect. Error bars correspond to the rms of the fit: 26.0 km s$^{-1}$ for the primary ( *filled circles*) and 28.0 km s$^{-1}$ for the secondary (*open circles*).

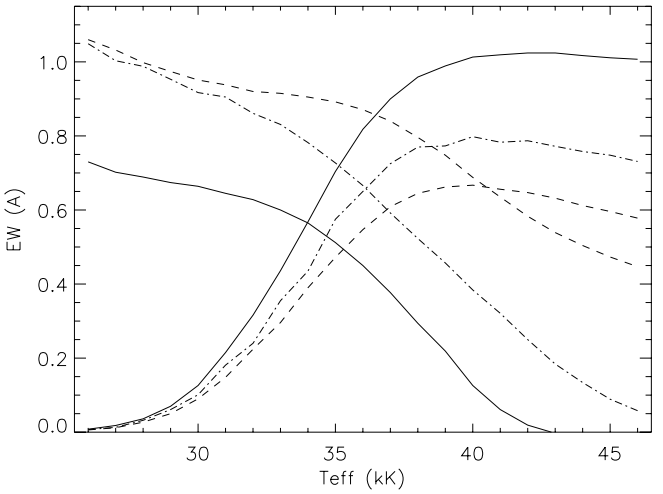



FIG. 5.—Equivalent widths of helium lines vs. $T_{\rm eff}$. The He I line strengths decrease with increasing $T_{\rm eff}$ (*solid line*: $\lambda$4921; *dashed-dotted line*: $\lambda$4471; *dashed line*: $\lambda$4026); the He II line strengths increase (*solid line*: $\lambda$5411; *dashed-dotted line*: $\lambda$4542; *dashed line*: $\lambda$4200).

### 3.4. *Determination of Effective Temperatures*

The effective temperatures of the stars were determined by fitting the observed spectra with FASTWIND spectra. We adopted solar metallicity in the models appropriate for a deprojected galactocentric radius of 460″ for the DEB, according to Zaritsky et al. (1989) and Urbaneja et al. (2005). The value of log ($g$) and the flux ratio were both fixed to the values found from the analysis of the light and radial velocity curves (see § 3.3). We used $v_{\rm turb} = 0$ as appropriate (see Repolust et al. 2004) and $N({\rm He})/N({\rm H}) = 0.1$, the measured $v \sin i$ of 120 km s$^{-1}$, and adopted values for the mass-loss rates of $\dot{M} = 6.7 \times 10^{-7}$ for the primary and $1.7 \times 10^{-7}\ M_\odot\ {\rm yr}^{-1}$ for the cooler secondary. This choice of mass-loss rates is justified by the fit of the mass-loss-dependent He II line $\lambda$4686 (see Repolust et al. 2005; Massey et al. 2004, 2005), shown in Figure 8. It also agrees with the average values found by Repolust et al. (2005) for stars of similar parameters. The terminal velocities of the stellar wind are correlated with the photospheric escape velocities. Following Kudritzki & Puls (2000), we adopted for the former 2200 and 2600 km s$^{-1}$.

We combined spectra near quadratures (phases 0.26 and 0.68) with similar radial velocities, degrading the ESI spectra to match GMOS resolution and dispersion where appropriate. The difference in the velocities is between 0 and 60 km s$^{-1}$, which corresponds to a maximum shift of 0.9 Å in our wavelength range and does not affect the temperature determination. We fit composite model spectra to all the helium lines in our wavelength range except He I $\lambda$4713, which was too noisy to use quantitatively. However, the fits were in agreement with this line as well. The composite spectra were calculated as follows:

$$F_\lambda = w_1 F_{1,\lambda}(T_1) + w_2 F_{2,\lambda}(T_2) \qquad (2)$$

where

$$w_1 = \frac{1}{1 + (R_2/R_1)^2 F_2/F_1} \text{ and } w_2 = 1 - w_1 \qquad (3)$$

and where $F_1$ and $F_2$ are the normalized spectra for the primary and the secondary, respectively.The ratio of the radii and fluxes were fixed to the values derived in the previous section, therefore the only free parameter was $T_1$. The He II $\lambda$4542/He I $\lambda$4471 ratio measured from the spectra indicated a spectral type of O7 for both

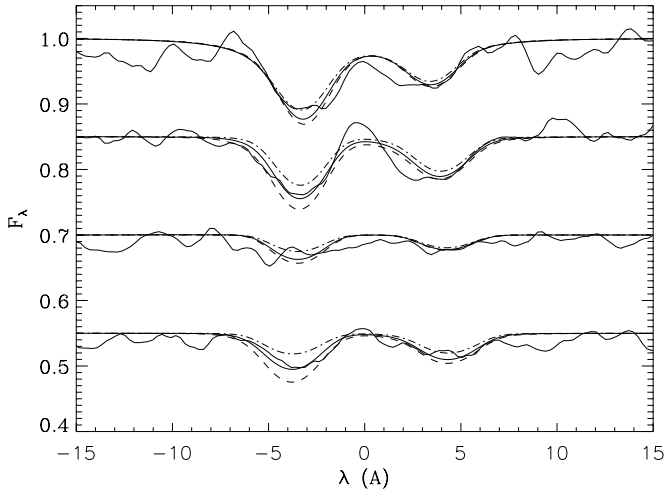



FIG. 6.—Fit of the composite spectra of He I lines at phase 0.26. At this phase the absorption lines originating in the primary are blueshifted, whereas the lines from the secondary are redshifted. Rectified spectra corrected for the gamma velocity are plotted as a function of wavelength displacement from the atomic line transition wavelength. The lines from top to bottom are He I $\lambda\lambda$4026, 4471, 4713, and 4921, and have been shifted in flux by 0.15 for clarity. Overplotted are the model calculations as described in the text. The solid curve represents our final model corresponding to a primary effective temperature of 37,000 K. The dashed and the dashed-dotted curves represent primary temperatures of 39,000 and 35,000 K, respectively.

stars. In this regime the helium line strengths are quite sensitive to temperature. The He II line equivalent widths increase with increasing effective temperature, whereas the He I widths decrease. Figure 5 illustrates this dependence for several lines. Finally, we resolved the degeneracy in the radii from the information in the spectra by determining that the slightly hotter primary contributes twice as much light, thus forcing it to be the larger star.

The temperature of the primary was derived from a simultaneous fit to the following seven lines: He I $\lambda\lambda$4026, 4388, 4471, 4921 and He II $\lambda\lambda$4200, 4542, 4686. Figures 6, 7, and 8 show fits to the helium lines at each quadrature. The fits to the Balmer lines shown in Figures 9 and 10 demonstrate that the model atmospheres reproduce the spectra correctly with the gravities derived from the light- and radial velocity curve analysis. The strong emission lines in the center of the hydrogen and some of the helium lines originate in nearby H II regions. The effective temperature of the

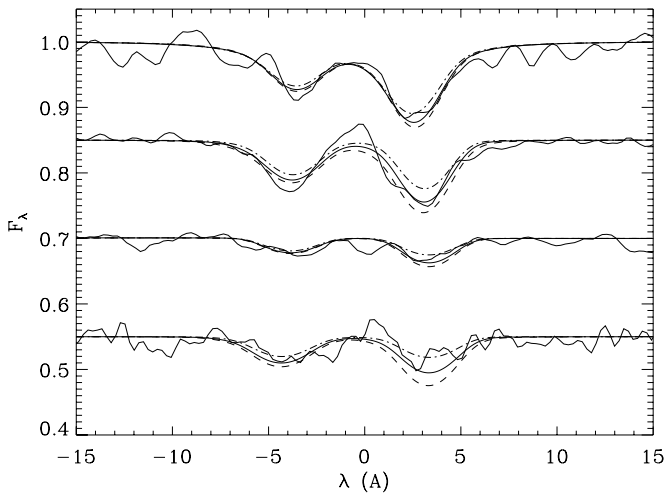



FIG. 7.—Same as Fig. 6, but at phase 0.68, where the lines from the primary (secondary) are redshifted (blueshifted).

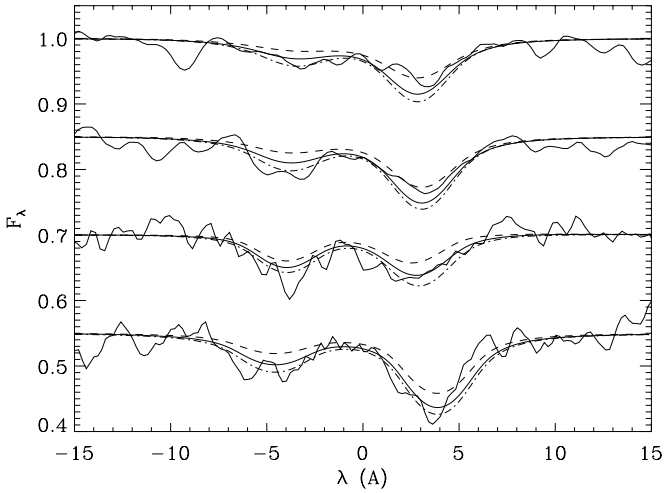



FIG. 8.—Same as Fig. 7, but for the He II lines. Plotted are He II $\lambda\lambda$4200, 4542, 4686, and 5411 (*top to bottom*).

secondary follows from the flux ratio and is consistent with the spectral fit of the lines from the secondary as displayed in the figures. We found the best-fit temperature for all the helium lines to be $T_{\rm eff,1} = 37{,}000 \pm 1500$ and consequently $T_{\rm eff,2} = 35{,}600 \pm 1500$ K.

## 4. DISTANCE DETERMINATION

The flux $f_\lambda$ measured at Earth at a certain wavelength $\lambda$ from a binary at distance $d$ is given by

$$f_\lambda = \frac{1}{d^2}\left(R_1^2 F_{1,\lambda} + R_2^2 F_{2,\lambda}\right) \times 10^{-0.4A(\lambda)}, \tag{4}$$

where $R_1$ and $R_2$ are the radii of the two stars, and $F_{1,\lambda}$ and $F_{2,\lambda}$ the surface fluxes. The total extinction $A(\lambda)$ is a function of the reddening $E(B-V)$, the normalized extinction curve $k(\lambda - V) \equiv E(\lambda - V)/E(B-V)$, and the ratio of total to selective extinction in the $V$ band $R \equiv A(V)/E(B-V)$:

$$A(\lambda) = E(B-V)[k(\lambda - V) + R]. \tag{5}$$

Having measured the temperatures of the stars from the spectra, we computed fluxes and fit to the observed magnitudes, using equation (4) and FASTWIND model atmospheres with

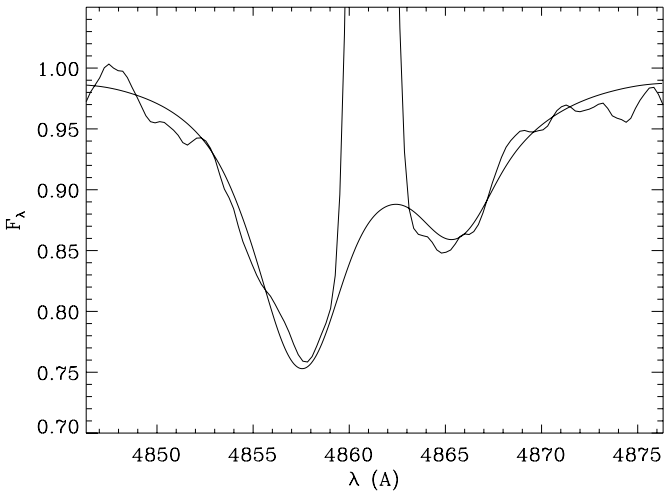



FIG. 9.—Plot of the H$\beta$ profile at phase 0.26 compared to the final model.

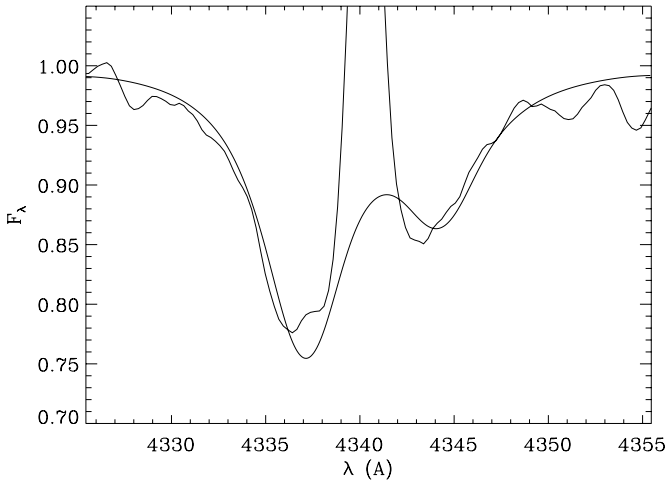



FIG. 10.—Same as Fig. 9, but for H$\gamma$.

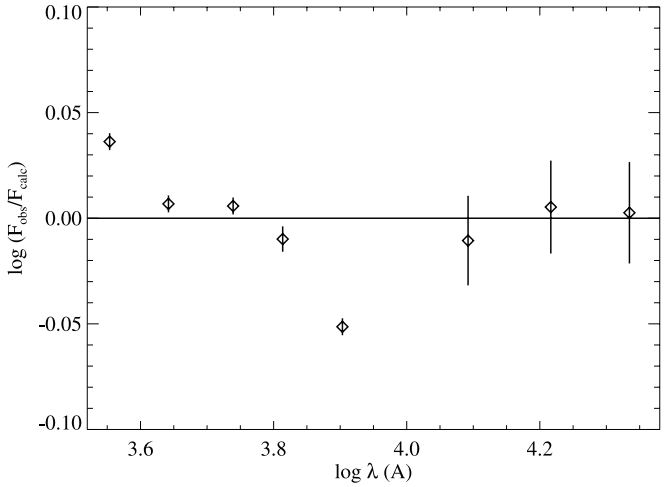



FIG. 12.—Residuals of the SED fit, in terms of the flux ratio. The error in the fit to the *BVRJHK$_s$* photometry corresponds to 0.01 mag. *U* and *I* are shown but not used in the fit. Error bars correspond to the photometric error for each band in flux units.

$T_{\rm eff,1} = 37{,}000$ and $T_{\rm eff,2} = 35{,}000$ K. We calculated synthetic photometry of the composite spectrum over the appropriate Johnson-Cousins optical filter functions as defined by Bessell (1990) and calibrated by Landolt (1992) and the 2MASS filter set. Monochromatic fluxes were measured at the isophotal wavelengths (see Tokunaga & Vacca 2005), which best represent the flux in a passband. We used zero points from Bessell et al. (1998; Appendix A) and from Cohen et al. (2003) to convert the fluxes to magnitudes. We reddened the model spectrum using the reddening-law parameterization of Cardelli et al. (1989) as prescribed in Schlegel et al. (1998) and simultaneously fit the optical and near-infrared *BVRJHK$_s$* photometry. Specifically, we computed the intrinsic $(B - V)_0 = -0.29$ from the model atmospheres at the isophotal wavelengths, thus yielding $E(B - V) = 0.09 \pm 0.01$. The best fit that minimized the photometric error over the six photometric bands was given by $R_V = 3.5 \pm 0.5$. The resulting distance modulus to the DEB and thus M33 is $24.92 \pm 0.12$ mag ($964 \pm 54$ kpc). The fit of the reddened model spectrum to the photometry is shown in Figure 11, and the residuals in Figure 12. The *U*- and *I*-values from Massey et al. (2006) are shown but not used in the fit because there are inherent problems with *U*-band photometry (see discussion in Massey 2002) and the *I* band often suffers from fringing effects. The *BVR* photometry alone, assuming $R_V = 3.1$ and $E(B - V) = 0.09$, yields a distance modulus of 24.95 mag, demonstrating the consistency of the near-infrared with the optical photometry.

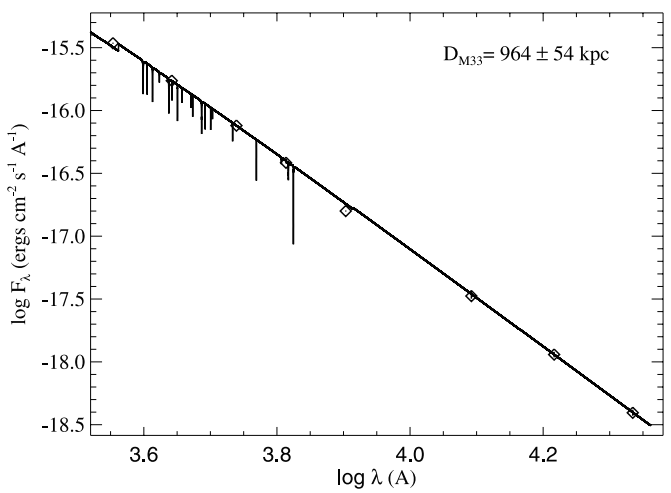



FIG. 11.—Fit of the reddened DEB model spectrum to the *BVRJHK$_s$* ground-based photometry. Overplotted is the *U* and *I* photometry from Massey et al. (2006). The best-fit values of $E(B - V) = 0.09 \pm 0.01$ and $R_V = 3.5 \pm 0.5$ yield a distance modulus to the DEB and thus M33 of $24.92 \pm 0.12$ mag ($964 \pm 54$ kpc).

The uncertainty in the distance was computed by adding in quadrature the individual conservative errors: 4% in the radii, which translates to 0.085 mag in the distance modulus, 4% in $T_{\rm eff,1}$ which corresponds to 0.06 mag, 0.04 mag from the SED fit, assuming $R_V = 3.5 \pm 0.5$ and $E(B - V) = 0.09 \pm 0.01$, and 0.03 mag in the flux. The error in the flux results from adding in quadrature the statistical 0.01 mag uncertainty from the fit to *BVRJHK$_s$* and the 0.03 mag uncertainty in the zero points. The total uncertainty is thus 0.12 mag. We did not attempt a full statistical treatment, since the error is dominated by the uncertainty in the radii. Note, that at these high temperatures the $B - V$ color of stars saturates, giving a weak dependence of the distance modulus on $T_{\rm eff}$.

As an independent check on our reddening and extinction determination we used CHORIZOS (Maíz-Apellániz 2004). We first generated a grid of TLUSTY models (Lanz & Hubeny 2003) at solar metallicity in the temperature and gravity regime of interest and fixed the effective temperature to 37,000 K and $\log(g) = 3.80$. The $\chi^2$ minimization fit to the *BVJHK$_s$* photometry resulted in $R_{5495} = 3.7 \pm 0.5$ and $E(4405 - 5495) = 0.07 \pm 0.01$, in agreement with the FASTWIND analysis. Note, that we computed these values at the isophotal wavelengths, which are bluer. We adopted these errors in the error analysis above.

## 5. DISCUSSION

We present the first distance to a detached eclipsing binary in M33, establishing it as an independent rung on the cosmological distance ladder. This distance determination is a significant step toward replacing the current anchor galaxy of the extragalactic distance scale, the LMC, with galaxies more similar to those in the *HST* Key Project (Freedman et al. 2001), such as M33 and M31. We have chosen a detached eclipsing binary to simplify the modeling and derived a distance modulus of $24.92 \pm 0.12$ mag.

D33 J013346.2+304439.9 is located in the rich OB 66 association (Humphreys & Sandage 1980), which contains a relatively high massive star population (Massey et al. 1995). The presence of one of the best-candidate detached eclipsing binaries

TABLE 7
Recent Distance Determinations to M33

| Study | Method[a] | Distance Modulus | Reddening |
|---|---|---|---|
| This work | DEB | $24.92 \pm 0.12$ | $E(B-V) = 0.09 \pm 0.01$ |
| Sarajedini et al. (2006) | RR Lyrae | $24.67 \pm 0.08$ | $\sigma_{E(V-I)} = 0.30$ |
| Brunthaler et al. (2005) | Water masers | $24.32 \pm 0.45$ | ... |
| Ciardullo et al. (2004) | PNe | $24.86^{+0.07}_{-0.11}$ | $E(B-V) = 0.04$ |
| Galleti et al. (2004) | TRGB | $24.64 \pm 0.15$ | $E(B-V) = 0.04$ |
| McConnachie et al. (2004) | TRGB | $24.50 \pm 0.06$ | $E(B-V) = 0.042$ |
| Tiede et al. (2004) | TRGB | $24.69 \pm 0.07$ | $E(B-V) = 0.06 \pm 0.02$ |
| Kim et al. (2002) | TRGB | $24.81 \pm 0.04(r)^{+0.15}_{-0.11}(s)$ | $E(B-V) = 0.04$ |
| | RC | $24.80 \pm 0.04(r) \pm 0.05(s)$ | $E(B-V) = 0.04$ |
| Lee et al. (2002) | Cepheids | $24.52 \pm 0.14(r) \pm 0.13(s)$ | $E(B-V) = 0.20 \pm 0.04$ |
| Freedman et al. (2001) | Cepheids | $24.62 \pm 0.15$ | $E(V-I) = 0.27$ |
| Pierce et al. (2000) | LPVs | $24.85 \pm 0.13$ | $E(B-V) = 0.10$ |
| Sarajedini et al. (2000) | HB | $24.84 \pm 0.16$ | $\langle E(V-I) \rangle = 0.06 \pm 0.02$ |

[a] DEB: detached eclipsing binary; TRGB: tip of the red giant branch; PNe: planetary nebulae; RC: the red clump; LPVs: long-period variables; HB: horizontal-branch stars.

for distance determination in this association is not surprising. In addition to the DEB, OB 66 contains several other eclipsing binaries (see Paper VI), which suggests a high binary star formation rate for massive stars. Our adopted color excess value $E(B-V) = 0.09 \pm 0.01$ is smaller than estimations from Massey et al. (1995) for OB 66. Using the "$q$ method" and $UBV$ photometry of 36 stars, they derive $E(B-V) = 0.15 \pm 0.02$, and their spectroscopic sample yields $E(B-V) = 0.13 \pm 0.01$. However, our multiband photometry combined with the spectroscopy determines the reddening accurately; thus, it is unlikely our distance estimation suffers from systematic errors due to reddening.

There are several avenues for improving the distance to M33 and M31 using eclipsing binaries. Wyithe & Wilson (2002) propose the use of semidetached eclipsing binaries to be just as good or better distance indicators as detached eclipsing binaries, which have been traditionally considered to be ideal. The use of new improved stellar atmosphere models to derive surface brightnesses versus calibrations based on interferometry removes the restriction to DEBs for distance determination. In addition, Wyithe & Wilson (2002) outline other benefits for using semidetached binaries: their orbits are tidally circularized and their Roche lobe–filling configurations provide an extra constraint in the parameter space, especially for complete eclipses ($i \sim 90^\circ$). Bright semidetached binaries in M33 or M31 are not as rare as DEBs and are easier to follow up spectroscopically, as demonstrated by Ribas et al. (2005) in M31. Thus, for the determination of the distances to M33 and M31 to better than 5%, we suggest both determining distances to other bright DEBs and to semidetached systems found by DIRECT and other variability surveys. Additional spectroscopy of the DEB would also improve the current distance determination to M33, since the errors are dominated by the uncertainty in the radius or velocity semiamplitude.

How does our M33 distance compare to previous determinations? Table 7 presents a compilation of 13 recent distance determinations to M33, ranging from 24.32 to 24.92 mag, including the reddening values used. Our measurement, although completely independent, yields the largest distance with a small 6% error and thus is not consistent with some of the previous determinations. This possibly indicates unaccounted sources of systematic error in the calibration of certain distance indicators.

The implications of our result on the extragalactic distance scale are significant, especially when comparing to the *HST* Key Project (Freedman et al. 2001) distance to M33. They derive a metallicity-corrected Cepheid distance of $24.62 \pm 0.15$ mag, using a high reddening value of $E(V-I) = 0.27$ and an assumed LMC distance modulus of $18.50 \pm 0.10$ mag. If we calculate the LMC distance that our result would imply, we derive $18.80 \pm 0.16$ mag, which is not consistent with the eclipsing binary determinations. The error is obtained by adding in quadrature the individual errors in the two distance measurements. Taking this one step further, our LMC distance would imply a 15% decrease in the Hubble constant to $H_0 = 61$ km s$^{-1}$ Mpc$^{-1}$. This improbable result brings into question the Key Project metallicity corrections and reddening values not only for M33 but also for the other galaxies in the Key Project. We thus demonstrate the importance of accurately calibrating the distance scale and determining $H_0$, which are both vital for constraining the dark-energy equation of state (Hu 2005) and complementing the cosmic microwave background measurements from the *Wilkinson Microwave Anisotropy Probe* (*WMAP*; Spergel et al. 2006).

We are very grateful to Bohdan Paczyński for motivating us to undertake this project almost a decade ago. We thank Phil Massey for sending us his photometry of the DEB from his Local Group Survey before publication. We would like to thank the staff of the Mount Hopkins Observatory for their support during extensive observing campaigns and the anonymous referee for comments that improved the manuscript. A. Z. B. and K. Z. S. were partially supported by *HST* grant HST-GO-09810.06-A. A. Z. B. acknowledges research and travel support from the Carnegie Institution of Washington through a Vera Rubin Fellowship. Support for L. M. M. was provided by NASA through Hubble Fellowship grant HST-HF-01153 from the Space Telescope Science Institute and by the NSF through a Goldberg Fellowship from the National Optical Astronomy Observatory. J. K. was supported by MNiI grant 1P03D001-28. B. J. M. was supported by the Polish KBN grant 1P03D01230. G. T. acknowledges partial support from NSF grant AST 04-06183.

Some of the data presented herein were obtained at the W. M. Keck Observatory, which is operated as a scientific partnership among the California Institute of Technology, the University of California, and the National Aeronautics and Space Administration (NASA). The Observatory was made possible by the generous financial support of the W. M. Keck Foundation. The authors wish to recognize and acknowledge the very significant cultural role and reverence that the summit of Mauna Kea has

always had within the indigenous Hawaiian community. We are most fortunate to have the opportunity to conduct observations from this mountain. This paper is also based on observations obtained under Program ID GN-2004B-Q-25 and GN-2005B-DD-4 at the Gemini Observatory, which is operated by the Association of Universities for Research in Astronomy, Inc., under a cooperative agreement with the NSF on behalf of the Gemini partnership: the NSF (United States), the Particle Physics and Astronomy Research Council (United Kingdom), the National Research Council (Canada), CONICYT (Chile), the Australian Research Council (Australia), CNPq (Brazil) and CONICET (Argentina). This publication makes use of data products from the Two Micron All Sky Survey, which is a joint project of the University of Massachusetts and the Infrared Processing and Analysis Center, California Institute of Technology, funded by NASA and the NSF.

REFERENCES

Alard, C. 2000, A&AS, 144, 363
Alard, C., & Lupton, R. H. 1998, ApJ, 503, 325
Andersen, J. 1991, A&A Rev., 3, 91
Benedict, G. F., et al. 2002, AJ, 123, 473
Bessell, M. S. 1990, PASP, 102, 1181
Bessell, M. S., Castelli, F., & Plez, B. 1998, A&A, 333, 231
Bonanos, A. Z., et al. 2003, AJ, 126, 175
Brunthaler, A., et al. 2005, Science, 307, 1440
Cardelli, J. A., Clayton, G. C., & Mathis, J. S. 1989, ApJ, 345, 245
Ciardullo, R., et al. 2004, ApJ, 614, 167
Claret, A. 2000, A&A, 363, 1081
Cohen, M., Wheaton, W. A., & Megeath, S. T. 2003, AJ, 126, 1090
Fitzpatrick, E. L., et al. 2003, ApJ, 587, 685
Freedman, W. L., et al. 2001, ApJ, 553, 47
Galleti, S., Bellazzini, M., & Ferraro, F. R. 2004, A&A, 423, 925
Guinan, E. F., et al. 1998, ApJ, 509, L21
Harmanec, P., et al. 1997, A&A, 319, 867
Harries, T. J., Hilditch, R. W., & Howarth, I. D. 2003, MNRAS, 339, 157
Hilditch, R. W. 1996, in ASP Conf. Ser. 90, The Origins, Evolution, and Destinies of Binary Stars in Clusters, ed. E. F. Milone & J.-C. Mermilliod (San Francisco: ASP), 207
———. 2001, An Introduction to Close Binary Stars (Cambridge: Cambridge Univ. Press), 392
Hilditch, R. W., Howarth, I. D., & Harries, T. J. 2005, MNRAS, 357, 304
Hodapp, K. W., et al. 2003, PASP, 115, 1388
Hook, I., et al. 2003, Proc. SPIE, 4841, 1645
Hu, W. 2005, in ASP Conf. Ser. 339, Observing Dark Energy, S. C. Wolff & T. R. Lauer (San Francisco: ASP), 215
Humphreys, R. M., & Sandage, A. 1980, ApJS, 44, 319
Ilijic, S., Hensberge, H., & Pavlovski, K. 2001, Fizika B, 10, 357
Ilijic, S., et al. 2004, in ASP Conf. Ser. 318, Spectroscopically and Spatially Resolving the Components of the Close Binary Stars, ed. R. W. Hidlitch, H. Hensberge, & K. Pavlovski (San Francisco: ASP), 111
Ivanov, G. R., Freedman, W. L., & Madore, B. F. 1993, ApJS, 89, 85
Kallrath, J., & Milone, E. F. 1999, Eclipsing Binary Stars: Modeling and Analysis (New York: Springer)
Kaluzny, J., et al. 1998, AJ, 115, 1016
———. 1999, AJ, 118, 346
Kim, M., et al. 2002, AJ, 123, 244
Kruszewski, A., & Semeniuk, I. 1999, Acta Astron., 49, 561
Kudritzki, R., & Puls, J. 2000, ARA&A, 38, 613
Kurtz, M. J., et al. 1992, in ASP Conf. Ser. 25, Astronomical Data Analysis Software and Systems I, ed. D. M. Worrall, C. Biemesderfer, & J. Barnes (San Francisco: ASP), 432
Kurucz, R. 1993, CD-ROM 13, ATLAS9 Stellar Atmosphere Programs and 2 km/s Grid (Cambridge: Smithsonian Astrophys. Obs.), 13
Landolt, A. U. 1992, AJ, 104, 340
Lanz, T., & Hubeny, I. 2003, ApJS, 146, 417
Lee, M. G., et al. 2002, ApJ, 565, 959
Macri, L. M., et al. 2001, AJ, 121, 870 (Paper VI)
Maíz-Apellániz, J. 2004, PASP, 116, 859
Massey, P. 2002, ApJS, 141, 81
Massey, P., Bianchi, L., Hutchings, J. B., & Stecher, T. P. 1996, ApJ, 469, 629
Massey, P., et al. 1995, AJ, 110, 2715
———. 2004, ApJ, 608, 1001
———. 2005, ApJ, 627, 477
———. 2006, AJ, 131, 2478
Matheson, T., et al. 2000, AJ, 120, 1499
McConnachie, A. W., et al. 2004, MNRAS, 350, 243
Mochejska, B. J., et al. 1999, AJ, 118, 2211
———. 2000, AJ, 120, 810
———. 2001a, AJ, 121, 2032 (Paper VII)
———. 2001b, AJ, 122, 2477
———. 2001c, preprint (astro-ph/0103440)
Nelson, B., & Davis, W. D. 1972, ApJ, 174, 617
Paczynski, B. 1997, in The Extragalactic Distance Scale, ed. M. Livio, M. Donahue, & N. Panagia (Cambridge: Cambridge Univ. Press), 273
Pierce, M. J., Jurcevic, J. S., & Crabtree, D. 2000, MNRAS, 313, 271
Popper, D. M., & Etzel, P. B. 1981, AJ, 86, 102
Press, W. H., et al. 1992, Numerical Recipes in FORTRAN. The Art of Scientific Computing (2nd ed.; Cambridge: Cambridge University Press)
Puls, J., et al. 2005, A&A, 435, 669
Pych, W. 2004, PASP, 116, 148
Repolust, T., Puls, J., & Herrero, A. 2004, A&A, 415, 349
Repolust, T., et al. 2005, A&A, 440, 261
Ribas, I., et al. 2005, ApJ, 635, L37
Santolaya-Rey, A. E., Puls, J., & Herrero, A. 1997, A&A, 323, 488
Sarajedini, A., et al. 2000, AJ, 120, 2437
———. 2006, AJ, 132, 1361
Schlegel, D. J., Finkbeiner, D. P., & Davis, M. 1998, ApJ, 500, 525
Schwarzenberg-Czerny, A. 1989, MNRAS, 241, 153
———. 1996, ApJ, 460, L107
Sheinis, A. I., et al. 2002, PASP, 114, 851
Simon, K. P., & Sturm, E. 1994, A&A, 281, 286
Spergel, D. N., et al. 2006, ApJ, submitted (astro-ph/0603449)
Stanek, K. Z., et al. 1998, AJ, 115, 1894
———. 1999, AJ, 117, 2810
Stetson, P. B. 1987, PASP, 99, 191
———. 1990, PASP, 102, 932
Tiede, G. P., Sarajedini, A., & Barker, M. K. 2004, AJ, 128, 224
Tokunaga, A. T., & Vacca, W. D. 2005, PASP, 117, 421
Tonry, J., & Davis, M. 1979, AJ, 84, 1511
Urbaneja, M.-A., et al. 2005, ApJ, 635, 311
van Hamme, W. 1993, AJ, 106, 2096
van Hamme, W., & Wilson, R. E. 2003, in ASP Conf. Ser. 298, GAIA Spectroscopy: Science and Technology, ed. U. Munari (San Francisco: ASP), 323
Wade, R. A., & Horne, K. 1988, ApJ, 324, 411
Wilson, R. E. 1979, ApJ, 234, 1054
———. 1990, ApJ, 356, 613
Wilson, R. E., & Devinney, E. J. 1971, ApJ, 166, 605
Wyithe, J. S. B., & Wilson, R. E. 2002, ApJ, 571, 293
Zaritsky, D., Elston, R., & Hill, J. M. 1989, AJ, 97, 97
Zucker, S., & Mazeh, T. 1994, ApJ, 420, 806